An Analytical Model of Anisotropic Charged Strange Star and Prediction of Mass Admitting MIT Bag Equation of State

S. Sarkar¹

¹Department of Physics, Coochbehar Panchanan Barma University, Vivekananda Street, District: Coochbehar, Pin:736101, West Bengal, India

Publication Date: 2025/10/10

Abstract: In this study, we investigate the relativistic star model while accounting for pressure anisotropy. Anisotropic solution to Einstein equation has been pro- posed for strange quark stars using the inner space time geometry defined by the metric component $g_{tt} = H(1+x)^n$, where n is a parameter. Taking into account the equation of state for strange matter, expressed $P_r = \frac{1}{3}(\rho - 4B_g)$, where B_g is referred to as the Bag constant with in the framework of the MIT Bag model, we have successfully derived a stellar model. We posit the surface value of energy density to be $\rho_s=4B_g$. By establishing the constraint value of B_g with in the interval of 57.55- $95.11 MeV/fm^3$, which is requisite for the stability of quark matter in comparison to neutron matter at zero external pressure, we have conducted an assessment of the maximum mass and radius of strange quark star along with other pertinent characteristics. The investigation reveals that when the bag constant equals $B_g = 57.55 \text{ MeV/fm}^3$, the corresponding maximum stellar mass reaches $M_{max}=2.38M_{\odot}$ with a maximum radius of $b_{max}=13.21$ km. Conversely, when the bag constant increases to $B_g=95.11~MeV/fm^3$, the maximum achievable mass decreases to $M_{max}=1.85~M_{\odot}$ while the maximum radius reduces to $b_{max}=10.27km$ for the isotropic stellar configuration. When pressure anisotropy is present, the maximum mass value demonstrates an increase. Based upon our theoretical frame work, we have predicted the radii of recently detected pulsars and secondary celestial bodies observed in gravitational wave events GW170817 and GW190814. The current theoretical model satisfies all requisite energy conditions.

Keywords: General Relativity. Theoretical Astrophysics. Einstein Equations. Compact Stars.

How to Cite: S. Sarkar (2025) An Analytical Model of Anisotropic Charged Strange Star and Prediction of Mass Admitting MIT Bag Equation of State. *International Journal of Innovative Science and Research Technology*, 10(9), 2811-2825. https://doi.org/10.38124/ijisrt/25sep1255

I. INTRODUCTION

Over the past several decades, researchers in relativistic astrophysics have demonstrated considerable interest in the investigation of compact objects, establishing this field as a prominent area of scientific inquiry. Numerous endeavors have been undertaken to obtain exact solutions to Einstein's field equations and subsequently apply these solutions to characterize the structural composition of extremely dense compact objects. These compact objects represent the final evolutionary stage of stellar systems and are therefore classified as stellar remnants. Because of their extraordinary density characteristics, it is postulated that the internal structure of such stellar objects likely consists of exotic matter configurations, particularly within the central core

regions. Within neutron stars, the extreme conditions of temperature and pressure may facilitate the formation of a theoretical matter phase termed quark matter. Under sufficiently elevated pressure conditions, certain quarks under got transformation into strange quarks ,and the subsequent interactions between strange quarks and non strange quarks result in the formation of strange matter. Consequently, the presence of strange quark matter, particularly within the central regions of neutron stars and other ultra dense stellar objects, may significantly contribute to our comprehension of the observable physical properties exhibited by such celestial bodies. These astronomical objects are designated as strange stars SS and constitute a distinct classification within the strange star family. The conventional neutron star models currently available prove inadequate for elucidating the

observed characteristics of such celestial bodies, as these theoretical frameworks fail to provide accurate predictions regarding the precise evidence of these objects. The incorporation of strange quark matter theory presents a potentially valuable approach for investigating the physical properties of such astronomical entities. Within this theoretical framework, the MIT Bag model(1);(2);(3);(4);(5) may serve as an effective mechanism for deriving pertinent characteristics of quark matter. This particular model operates under the assumption that the constituent quark matter comprises mass less up (u) and down (d) quarks, alongside massive strange quarks (s) and electrons. Quarks are regarded as degenerate Fermi gases that can exist exclusively within spatial regions characterized by a vacuum energy density denoted as B_g , termed the Bag constant. Under the assumption that quarks possess zero mass and exhibit no mutual interactions, the quark pressure may be expressed as $p_q = \rho_q/3$, wherein ρ_q represents the energy density of the quarks. The total energy density and total pressure are characterized as,

$$\rho = \rho_q + B_g ,.... eq(1)$$

$$p = p_q - B_g$$
eq(2)

By eliminating the variables ρ_q and p_q from eqs.(1)and(2) and employing the relationship $p_q = \frac{1}{3}\rho_q$ it becomes possible to derive the equation of state (hereafter referred to as EOS) for mass less strange quark matter, as presented by Kapusta (6), which is expressed as,

$$p = \frac{1}{3}(\rho - 4B_g),...$$
eq(3)

Where B_g is mentioned earlier. Based on Madsen's theoretical framework (7), the parameter B_g exhibits specific constraints that are fundamental to maintaining the stability of strange matter configurations. The lower bound for this parameter has been established at $B^{1/4}=145 MeV$, corresponding to $B_g=57.55 MeV/fm^3$. Research (7) indicates that quark matter systems consisting exclusively of u and d quarks may exhibit inherent in stabilities. The incorporation of s quarks into the system serves to diminish the energy per baryon, consequently enhancing the overall stability of the configuration. For two flavor quark matter to demonstrate stability relative to neutrons, the energy per baryon must remain below the neutron mass threshold of (939.6 MeV), as established by Madsen(7), however, this condition is not manifested in naturally occurring systems. The stability of strange quarks, which is essential for maintaining stable strange matter in relation to neutrons under zero external pressure conditions, has been predicted by Madsen (7) and represents the minimum threshold value of B_g necessary to ensure atomic nuclei remain stable against decomposition into non strange quark matter, a phenomenon that is typically not observed experimentally. Conversely, the stability requirements of strange matter relative to iron establish

an upper limitation on B_g , specifically $B_{gmax}^{1/4}$ =162.8MeV, which corresponds equivalently to B_gmax = 91.54 MeV/fm^3 . Nevertheless, this maximum threshold changes to $Bg^{1/4}$ =164.4 MeV or its equivalent value of B_gmax = 95.11 MeV/fm^3 (7), at which point strange matter becomes stable compared to neutrons under conditions of zero external pressure. These threshold values are all calculated under zero external pressure conditions while disregarding quark- quark interactions (6;7). When the coupling constant is nonzero, both of these limiting values exhibit the anticipated reduction as theorized by Farhi (8).

https://doi.org/10.38124/ijisrt/25sep1255

During the initial phases of stellar structure modeling, researchers operated under the assumption that matter exhibited isotropic distribution properties. Nevertheless, this theoretical framework has been subsequently dismissed by numerous scholarly investigations, which demonstrated that such models failed to adequately account for the massradius relationships observed in compact stellar objects. A more accurate representation of stellar architecture can be achieved through the incorporation of anisotropic fluid distribution within the interior of compact objects. Numerous factors contribute to the development of anisotropic pressure within compact stellar objects. The theoretical prediction of pressure anisotropy existing with in such compact structures was initially proposed by Ruderman and Canuto (9)and(10). Research of Bowers(11) indicates that anisotropic properties may significantly influence the red-shift characteristics of anisotropic stellar bodies. The investigation by Kippenhahn (12) proposes that such anisotropic phenomena could originate from the existence of type 3A super fluid with in the central regions of compact astrophysical objects. Herrera and Santos(13) has provided a comprehensive examination of the potential mechanisms underlying pressure anisotropy in dense stellar remnants. For extremely dense stellar objects, the anisotropic characteristics can be elucidated through the influence of superconducting and super fluid phenomena (11). Additional potential mechanisms that may give rise to pressure anisotropy include pion condensation phenomena (14), phase transitions within the stellar medium (15), or the existence of a crystalline core structure within dense astrophysical objects. Many authors [(16); (17); (18)] has developed stellar model considering pressure anisotropy. Pressure anisotropy may also influence the stellar structure and physical characteristics (19),(20). Multiple studies [(21); (22); (23); (24); (25)] have established that anisotropic conditions can significantly affect fundamental stellar parameters, including the maximum allowable mass and stellar radius.

When electric charge is present, the gravitational collapse of a spherically symmetric celestial body toward a point singularity may potentially be prevented through Coulomb repulsive forces. Rosseland (27) initially theorized that stellar objects could harbor substantial quantities of electrons and positively charged ions. The

hypothesis suggests that electrons, possessing sufficient kinetic energy, may escape the stellar medium, resulting in the predominant presence of positive ions within the stellar structure. Consequently, these positively charged ions may contribute to the net electrical charge that exists within compact astrophysical objects. Within this framework, the theoretical modeling of compact objects in the presence of electrical charge has attracted considerable interest among researchers in the field. Therefore, in the domain of relativistic astrophysics, it becomes critically important to obtain solutions to Einstein's field equations when electric charge is present.

Bonnor (26) demonstrated that a spherically symmetric body can maintain hydrostatic equilibrium through the balance between gravitational attractive forces and the relatively weak Coulomb repulsive forces arising from the internal electric charge distribution. (28)demonstrated that fluid spheres possessing net electrical charge exhibit enhanced stability compared to uncharged stellar objects. The electromagnetic repulsive forces generated by the charge distribution serve to counterbalance gravitational attraction, thereby potentially preventing the formation of singularities (29). Several investigators have proposed that both the charged-dust (CD) theoretical framework and electromagnetic mass models may provide valuable insights into the fundamental structural properties of electrons [(30);(31); (32)]. Certain studies indicate that electrically charged fluid spheres exhibit greater physical significance compared to their uncharged counterparts (33). Numerous researchers have investigated charged anisotropic stellar models and determined their corresponding physical parameters (34), (35). The fundamental objective of this investigation is to develop and forecast an appropriate theoretical framework for compact celestial bodies in order to elucidate their empirically observed characteristics and the internal structural composition of their constituent matter.

This research examines a spherically symmetric electrically charged anisotropic strange star utilizing MIT EoS. This manuscript is structured as follows: Sect. 2, presents our analysis of the Einstein-Maxwell equations governing anisotropic charged stellar objects. Sect. 3, establishes the various criteria for physical acceptability. Sect. 4, introduces a new class of solutions to the Einstein field equations in the presence of electromagnetic charge. Sect. 5, examines the requisite boundary conditions for our model. Sect.6, derives the mass function, compactness parameter, and gravitational red shift function.Sect.7, employs the MIT bag model framework for our numerical computations. Sect. 8, investigates various physical parameters and their implications.Sect.9, shows energy conditions. Sect. 10, demonstrate causality criterion. Sect. 11, the application of our theoretical framework to two distinct stellar configurations. Sect.11, shows physical application of the model. Sect. 12, addresses multiple stability criteria and their verification. Finally, Sect. 13, provides a comprehensive summary of our findings and conclusions.

II. EINSTEIN-MAXWELL' SFIELDEOUATIONS

The metric tensor characterizing the internal space time geometry of a static, spherically symmetric stellar fluid configuration may be expressed in the following form:

$$ds^{2} = -e^{v(r)}dt^{2} + e^{\lambda(r)}dr^{2} + r^{2}(d\theta^{2} + \sin^{2}\theta d\phi^{2}) eq(4)$$

Here, v(r) and $\lambda(r)$ represent the metric potentials that exhibit dependence solely on the radial coordinate. In the context of an anisotropic charged matter configuration, the energy-momentum tensor T_{mn} may be formulated as follows:

$$T_{mn} = \text{diag}(-\rho - E^2, p_r - E^2, p_t + E^2, p_t + E^2), \dots eq(5)$$

Where ρ , p_r and p_t are respectively matter density, radial pressure and transverse pressure. The anisotropy in pressure $\Delta = (p_t - p_r)$. The renowned EFE is expressed as:

Where R_{mn} denotes the Ricci tensor while R represents the Ricci scalar. The energy-momentum tensor corresponding to the interior matter distribution is designated as T_{mn} . The coupling constant $k = \frac{8\pi G}{c^2}$ incorporates the Newtonian gravitational constant G. Within astrophysical conventions, it is customary to employ normalized units where G=1 and c=1. The fundamental physical parameters namely ρ , p_r and p_t may be derived through the solution of Einstein field equations as formulated in Eq.(6). By implementing the relationships established in Eqs.(4) and (5),the Einstein field equation presented in Eq.(6) yields the subsequent system of equations:

$$e^{-\lambda} \left(\frac{\lambda'}{r} - \frac{1}{r^2} \right) + \frac{1}{r^2} = k^2 \rho + E^2,$$
 eq(7)

$$e^{-\lambda} \left(\frac{v'}{r} + \frac{1}{r^2} \right) - \frac{1}{r^2} = k^2 p_r - E^2$$
, eq(8)

Using the relation $\Delta = (pt-pr)$ and putting the values of pr and pt from Eqs. (8) and (9) respectively, we obtain the following equation,

$$e^{-\lambda} \left[\frac{v''}{2} + \frac{{v'}^2}{4} - \frac{\lambda' v'}{4} - \frac{(\lambda' - v')}{2r} \right] = k^2 p_t + E^2.$$
 (9)

$$e^{-\lambda} \left[\frac{v''}{2} + \frac{{v'}^2}{4} - \frac{\lambda' v'}{4} - \frac{(\lambda' + v')}{2r} - \frac{1}{r^2} \right] + \frac{1}{r^2} = k^2 \Delta + 2E^2. \qquad eq(10)$$

Where the term $k=\frac{8\pi G}{c^2}$ and the prime notation denotes differentiation with respect to the radial

Volume 10, Issue 9, September – 2025

ISSN No:-2456-2165

coordinate r. The total mass enclosed within a spherical volume of radius r is expressed as follows,

$$m(r) = 4\pi \int_0^r r^2 \rho(r) dr....eq(11)$$

Where $\rho(\mathbf{r})$ is the matter density and is given in eq. (7). For maximum mass we have to use r = b, b is the maximum radius of the strange star.

III. PHYSICAL ACCEPTABILITY CONDITIONS

To achieve a well characterized and appropriate solution for the mathematical model, the following criteria must be fulfilled:

- The solution must remain free of singularities, requiring that the central density, central pressure and metric potentials $e^{-\lambda}$ and e^{ν} maintain finite and positive values throughout the system.
- The energy density and pressure in presence of charge and anisotropy pick up positive and monotonically decreasing values. This indicates that within the anisotropic charged fluid sphere, the gradients of both pressure and energy density must be negative as they vary with the radial coordinate *r* i.e.

$$\left(\frac{dp_r}{dr}\right) < 0, \left(\frac{dp_t}{dr}\right) < 0 \ and \ \left(\frac{d\rho}{dr}\right) < 0.$$

- The anisotropy factor Δ should be zero at the center and increasing away from the center.
- The electric field E² must be zero at the center of the star.
- The charge density is maximum at the center and decreases away from the center and attains minimum value at the surface.
- All the energy conditions should be satisfied with in the star.
- The sound speed must be less than 1 i.e.

$$0 \le \left(\frac{dp_r}{dp}\right) \le 1$$
 and $0 \le \left(\frac{dp_t}{dp}\right) \le 1$ inside the star.

• The compactness should be less than $\frac{4}{9}$ i.e. $\frac{M}{b} < \frac{4}{9}$, Buchdahal limit (36).

IV. A NEW CLASS OF SOLUTION OF EINSTEIN-MAXWELL EQUATION IN PRESENCE OF CHARGE AND PRESSURE ANISOTROPY

Equations (7)-(9) contain five unknowns: λ , ν , ρ , p_r and p_t . A viable stellar model requires determining ρ , p_r and p_t values. We must select appropriate metric potentials and from available astrophysical forms that satisfy all necessary conditions for viable stellar models. Here, we consider the g_{tt} metric component as:

$$e^{v} = H(1+x)^{n}, \dots eq(12)$$

Where x=hr² and n is a parameter. This particular metric configuration is employed due to its absence of singularities and its well regulated behavior across the entire interior region of the stellar system. This characteristic facilitates the derivation of well regulated solutions to the Einstein Field Equations. Through the systematic variation of the parameter n, one can generate an extensive array of exact analytical solutions. Numerous such solutions have previously been established by various researchers in the field.

- For *n*=1 the solution obtained by Durgapal which is identical to the Tolman IV solution (37).
- For n=2 the solution obtained by Durgapal is identical with the solution obtained by [(38), (39) and (40)].
- For n=3,4,5 the solutions and its physical features were studied by Durgapal (41).

Our objective now involves deriving the expression for the g_{rr} metric tensor component for n>5 by employing Eqs. (7) and (8), in conjunction with the pressure anisotropy relationship $\Delta = (p_t - p_r)$ and Eq. (12). Through the implementation of the coordinate transformations $e^{-\lambda} = Y(x)$ and $x = hr^2$, where in h represent constant whose magnitudes may be established via various boundary conditions and by utilizing Eq. (12), Eq. (10) undergoes the following transformation:

Where, ψ and \in are given as,

$$\psi = \frac{(n^2x^2 - 2nx^2 - (1+x)^2)}{x(x+1)(nx+x+1)}, \dots \dots eq(14)$$

$$\epsilon = \frac{(1+x)}{(nx+x+1)} \left[\frac{1}{x} - \frac{\Delta}{h} - \frac{2E^2}{h} \right], \dots \dots eq(15)$$

Where $\Delta = (p_t - p_r)$ is defined earlier.

➤ Isotropic Uncharged Solution for n=6

For anisotropic and uncharged solution, the equation eq. (13) reduces to

$$\frac{dY}{dx} + \psi Y + \epsilon = 0, \dots eq(16)$$

Where, ψ and \in are given as,

$$\psi = \frac{(24x^2 - (1+x)^2)}{x(x+1)(7x+1)}, \dots eq(17)$$

$$\in = \frac{(1+x)}{(7x+1)} \frac{1}{x} \dots eq(18)$$

The solution of eq. (16) gives the g_{rr} component of metric potential as,

$$e^{-\lambda} = \frac{1}{(1+x)^4} \left[1 - \frac{x^4 + 7x^3 + 24x^2 + 103x}{23} \right] + \frac{4x(1+7x)^{-\frac{2}{7}}}{(1+x)^4}. \text{ eq}(19)$$

Where A is a constant determined by boundary conditions. Now it is possible to find the different physical quantities relevant to the stellar configuration for an isotropic uncharged strange star viz density (ρ) , pressure (p), using the values of $e^{-\lambda}$ and e^{ν} . Hence an isotropic uncharged star may be obtained.

➤ Anisotropic Solution in Presence of Charge for n=6

To derive an anisotropic charged stellar model, it is essential to incorporate pressure anisotropy into our analysis. For the resolution of the differential equation presented in Eq. (13), it becomes necessary to select a mathematically well defined functional form for the parameters Δ and E^2 . Many authors [(17), (42), (43), (44), (45)] choose the pressure anisotropy and electric field in polynomial form to predict some viable result of stellar configuration. With this consideration, pressure anisotropy has been selected the configuration as follows,

$$\frac{\Delta}{h} = \frac{\alpha x (1+7x)^{-L/4}}{(1+x)^5} , \dots \dots eq(20)$$

This form of ensures that it is regular and well behaved inside the star. Also , Δ =0 at the center. The electric field E^2 is taken as:

$$\frac{E^2}{h} = \frac{\beta x (1+7x)^{-J/4}}{(1+x)^5} , \dots eq(21)$$

Such form of electric field is also regular and well behaved throughout the interior of the star. Also it is evident that at r=0, the electric field E^2 =0. The terms α and β are model parameters whose values are suitably chosen. Where, L and J are positive constants. Using Eqs. (20) and (21) with help of Eq. (17) and Eq. (18), the solution of Eq. (16) is obtained as:

$$e^{-\lambda} = \frac{1}{(1+x)^4} \left[1 - \frac{x^4 + 7x^3 + 24x^2 + 103x}{23} \right] +$$

$$\frac{4x(\frac{\alpha(1+7x)^{-\frac{L}{4}}}{(8-7L)} + \frac{2\beta(1+7x)^{-\frac{L}{4}}}{(8-7J)})}{(1+x)^4} + \frac{4x(1+7x)^{-\frac{2}{7}}}{(1+x)^4}....eq(22)$$

Where A is an arbitrary constant of integration and its value can be found from the different boundary conditions. A noteworthy observation is that Eq. (22) implies to the Durgapal VI th isotropic uncharged solution when α =0, β =0, as demonstrated in Eq.(19). Subsequently, we can calculate the physical parameters associated with the compact stellar object by utilizing the derived expressions for $e^{-\lambda}$ and e^{ν} as:

International Journal of Innovative Science and Research Technology https://doi.org/10.38124/ijisrt/25sep1255

$$\rho = -\frac{h\beta x (1+7x)^{-\frac{1}{4}}}{(1+x)^5} + \frac{h}{x} \left(1 - \frac{f_2}{(1+x)^4}\right) - 2h \left(\frac{f_1}{(1+x)^4} - \frac{4f_2}{(1+x)^5}\right), \dots eq(23)$$

$$p_r = \frac{h\beta x (1+7x)^{-\frac{1}{4}}}{(1+x)^5} - \frac{h}{x} - \frac{hf_2(1+13x)}{x(1+x)^5}, \dots eq(24)$$

$$p_{t=\Delta}, p_r, \dots eq(25)$$

And the charge density is obtained as:

$$\sigma = \frac{1}{4\pi} \sqrt{\frac{h}{x}} \frac{\sqrt{f_2 f_6}}{(1+x)^2} \left(2 + \frac{x f_7}{2}\right), \dots eq(26)$$

Where,

$$f_{1=} \frac{A(1+5x)}{(1+7x)^{9/7}} + \frac{(-4x^3 - 21x^2 - 48x - 103)}{23} + f_3 + f_4,$$

$$f_2 = f_5 + \frac{4\alpha x (1+7x)^{-\frac{L}{4}}}{(8-7L)} + \frac{8\beta x (1+7x)^{-\frac{J}{4}}}{(8-7J)},$$

$$f_3 = \frac{(1+7x)^{\left(-1-\frac{L}{4}\right)}(4+28x-7Lx)}{(8-7L)},$$

$$f_4 = \frac{(1+7x)^{\left(-1-\frac{J}{4}\right)}(8+56x-14Jx)}{(8-7J)},$$

$$f_5 = 1 + \frac{Ax}{(1+7x)^{\frac{2}{7}}} + \frac{-x^4-7x^3-24x^2-103x}{23},$$

$$f_6 = \frac{h\beta x (1+7x)^{-\frac{J}{4}}}{(1+x)^5},$$

$$f_7 = \left(\frac{(2-8x)}{x(1+x)} - \frac{7J}{2(1+7x)}\right).$$

In Eq. (12) and in Eqs. (23)-(26), the constants h, H and A can be obtained from the boundary conditions. At this juncture, we establish correspondence between the internal space time metric and the external space time metric at the boundary interface, where upon we, observe the subsequent conditions:

• We Know that for a Charged Star the Reissner-Nordstrom (47; 48) Exterior Metric is given by

$$ds^{2} = -\left(1 - \frac{2m}{r} + \frac{q^{2}}{r^{2}}\right)dt^{2} + \frac{dr^{2}}{\left(1 - \frac{2m}{r} + \frac{q^{2}}{r^{2}}\right)} + r^{2}d\Omega^{2}, \dots \dots eq(27)$$

Where $d\Omega^2{=}(d\theta^2{+}sin^2~\theta d\phi^2~),~q~$ is the charge inside the star of radius r and m being the mass of the star. Matching condition of metric potentials at the boundary r=b gives the following:

$$e^{\nu(r=b)} = e^{-\lambda(r=b)} = \left(1 - \frac{2M}{b} + \frac{Q^2}{b^2}\right) \dots \dots eq(28)$$

Using Eqs. (12), (22) and (28), we get

$$\left(1 - \frac{2M}{b} + \frac{Q^2}{b^2}\right) = \frac{1}{(1+X)^4} \left[1 - \frac{X^4 + 7X^3 + 24X^2 + 103X}{23}\right] +$$

$$\frac{4X(\frac{\alpha(1+7X)^{-\frac{L}{4}}}{(8-7L)} + \frac{2\beta(1+7X)^{-\frac{L}{4}}}{(8-7J)})}{(1+X)^4} + \frac{AX(1+7X)^{-\frac{2}{7}}}{(1+X)^4}, \dots eq(29)$$

And

$$H(1+X)^6 = \left(1 - \frac{2M}{b} + \frac{Q^2}{b^2}\right), \dots \dots \dots eq(30)$$

Where $X = hb^2$ and Q is the total charge within the sphere of radius b.

 The Radial Pressure which is a Decreasing Function of r Must Vanishes at the Surface of the Compact Object.
 i.e.

$$p_r(r = b) = 0....eq(31)$$

From Eqs. (29)- (31), we can determine the values of model constants and hence a viable model can be constructed.

V. BOUNDARY CONDITIONS OF THE MODEL

This section examines the constraints imposed upon the model parameters. Through application of the criterion established in Eq. (31),the parameter A can be determined and is presented as,

$$A = F_7 [63LF_5 + 4F_6 - 12744X + 1196X\alpha(1+7x)^{-\frac{L}{4}}, \dots eq(32)]$$

And the value of H is obtained as:

$$H = \frac{1}{(1+X)^{10}} \left[1 - \frac{X^4 + 7X^3 + 24X^2 + 103X}{23} \right] +$$

$$\frac{4X(\frac{\alpha(1+7X)^{-\frac{L}{4}}}{(8-7L)} + \frac{2\beta(1+7X)^{-\frac{L}{4}}}{(8-7J)})}{(1+X)^{10}} + \frac{AX(1+7X)^{-\frac{2}{7}}}{(1+X)^{10}}, \dots eq(33).$$

Where,

$$F_5 \!\!=\!\! (\text{-} \; 9 \!+\! 177X \!+\! 61X^2 \!+\! 23X^3 \!+\! 4X^4), \; F_6 \!\!=\!\! (162 \; \text{-} \; 1098X^2 \; \text{-} \; 414X^3 \\ \quad \text{-} \; 72X^4 \!+\! 23(1 \!+\! 7X)^{\text{-} \! L/4} \!\alpha \;)$$

And
$$F_7 = \frac{(1+7X)^{\frac{2}{7}}}{23(-8+7L)(1+13X)}$$
. Using Eqs. (21) and (30), we calculate the total mass of the compact object as:

International Journal of Innovative Science and Research Technology https://doi.org/10.38124/ijisrt/25sep1255

$$M = \frac{b}{2} \left(1 - H (1+X)^6 + \frac{X^2 \beta (1+7X)^{-\frac{J}{4}}}{(1+X)^5} \right) \dots \dots eq(34)$$

Central Density, Central Pressure and Central Charge Density

At r=0, we notice $(e^{\nu})_{r=0} = H$ and $(e^{-\lambda})_{r=0} = 1$ and their first derivatives $(e^{\lambda(r)})'_{r=0} = (e^{\nu(r)})'_{r=0} = 0$. This suggests that the metric potentials are regular and well behaved inside the star. The central density and pressure can be evaluated from Eqs. (23) and (24) at r=0 and are given below:

$$\rho(0) = \left(\frac{585}{23} - 3A - \frac{12\alpha}{(8 - 7L)} - \frac{24\beta}{(8 - 7I)}\right)h, \dots eq(35)$$

$$p_r(0) = \left(\frac{81}{23} + A + \frac{4\alpha}{(8-7L)} + \frac{8\beta}{(8-7I)}\right)h, \dots eq(36)$$

And the central charge density is obtained as:

$$\sigma(0) = \frac{3h\sqrt{\beta}}{4\pi} \dots eq(37)$$

As, $\sigma(0) > 0$, this suggests that h>0.

VI. MASS-RADIUS RELATIONSHIP, COMPACTNESS AND RED SHIFT FUNCTION

In this section, we calculate the mass contained within the sphere of radius r is given by the equation.

$$m(r) = 4\pi \int_0^r r^2 \rho \, dr....eq(38)$$

Where ρ is defined in Eq. (23). The compactness function is defined as u(r)=m(r)/r and the corresponding surface red-shift function is given as,

$$z(r) = \left(\frac{1}{\sqrt{1 - 2u(r)}} - 1\right) \dots \dots \dots \dots eq(39)$$

Fig.1 illustrates the relationship between stellar mass and radial distance from the center. The graphical representation demonstrates that the mass function exhibits regularity across the entire stellar interior. The boundary condition at the stellar center yields m(r= 0)=0. At the stellar boundary, a nonzero maximum gravitational red shift value has been observed. Fig. 2 presents the mass variation of the stellar object as a function of the parameter Bg for three distinct radial values: b=9Km, b=10Km and b=11Km.

VII. MAXIMUM MASS AND MAXIMUM RADIUS OF THE STAR

In this section, we calculate the probable maximum mass and maximum radius of the strange star taking MIT bag EOS. Here we use the numerical method to obtain the values of Mmax and bmax. The method is following:

- We calculate the maximum radius for a given surface value of energy density, ($\rho_s = 4Bg$) using Eq. (23), where B_g is bag constant.
- Initially we assume a radius b and using Eqs. (23) and (31) and for a particular value of α and β , we obtain the values of A and h.
- The choice of α and β are arbitrary but we should keep in mind that the radial pressure must be positive inside the star and becomes zero at the surface.
- Utilizing the determined values of A and h, the computation of the derivative $(\frac{dp_r}{d\rho})$ at the central point is performed. It is observed that a specific value of parameter b yields the maximum value of $(\frac{dp_r}{d\rho})$ at the center. This particular value of b, which corresponds to the maximum $(\frac{dp_r}{d\rho})$ at the center, represents the maximum permissible radius b_{max} for the strange star configuration given a specified surface energy density (ρ_s) or B_g parameter. The maximum mass corresponds to the mass of the compact stellar object encompassed within the radius b_{max} according to this theoretical

frame work and is determined through the expression $M_{max} = \frac{b_{max}}{2} (1 - e_{bmax}^{-\lambda} + E^2 b_{max}^2)$, where $e_{bmax}^{-\lambda}$ denotes the value of e^{λ} evaluated at the radial coordinate $r = b_{max}$.

In Tabs 1 and 3, we have shown the maximum mass and maximum possible radius of strange star for different values of α at Bg=57.55 MeV /fm³ and Bg= 95.11 MeV /fm ³ respectively. Tabs 2 and 4 show maximum mass and maximum possible radius of strange star for different values of β at Bg=57.55 MeV/fm³ and Bg= 95.11 MeV/fm³ From these tables, we notice that at $Bg = 57.55 MeV /fm^3$ the maximum mass is $M_{max}=2.67M_{\odot}$ at radius $b_{max}=13.54$ (km), where as at Bg=95.11MeV/ fm³ there values are M_{max} =2.08 M_{\odot} and b_{max} =10.53(km) for α =2.0 and β =0. Again, at $\alpha = 0$, we notice that at Bg = 57.55MeV/ fm³ the maximum mass is $M_{max}=3.23M_{\odot}$ at radius $b_{mx}=13.82$ (km), whereas at Bg =95.11MeV/ fm³ there values are M_{max} =2.51 M_{\odot} and b_{max} =10.75(km) for β =2.0. Tables 5 and 6 show the values of maximum compactness for different values of bag parameter Bg.

Table 1 Maximum Radius $b_{max}(Km)$ and Maximum Mass $M_{max}(M_{\odot})$ for $Bg = 575.5 MeV / fm^3$ taking L = 0.1, J = 0.3 and $\beta = 0$.

α	\boldsymbol{A}	H	$h(km^{-2})$	$b_{max}(km)$	$M_{max}(M_{\odot})$
0.0	1.97826	0.257892	0.000599	13.21	2.38
1.0	1.68032	0.22778	0.000654	13.39	2.53
2.0	1.38237	0.198633	0.000718202	13.54	2.67

Table 2 Maximum Radius $b_{max}(Km)$ and Maximum Mass $M_{max}(M_{\odot})$ for B_g =57.55 MeV/fm^3 taking L=0.1,J=0.3 and α =0.

β	A	Н	h(km-2)	b _{max} (km)	Mmax(Mo)
0.0	1.97826	0.257892	0.000599	13.21	2.38
1.0	1.20566	0.185942	0.000745	13.61	2.79
2.0	0.433065	0.12177	0.000971	13.82	3.23

Table 3 Maximum Radius $b_{max}(Km)$ and Maximum Mass $M_{max}(M\odot)$ for $B_g=95.11 MeV/fm^3$ taking L=0.1, J=0.3 and $\beta=0$.

α	\boldsymbol{A}	H	$h(km^{-2})$	$b_{max}(km)$	$M_{max}(M_{\bigodot})$
0.0	1.97826	0.257895	0.000990	10.27	1.85
1.0	1.68032	0.227791	0.0010803	10.41	1.97
2.0	1.38237	0.198633	0.00118694	10.53	2.08

Table 4 Maximum Radius $b_{max}(Km)$ and Maximum Mass $M_{max}(M\odot)$ for $B_g=95.11 MeV/fm^3$ taking L=0.1, J=0.3 and $\alpha=0$.

β	\boldsymbol{A}	H	$h(km^{-2})$	$b_{max}(km)$	$M_{max}(M_{\odot})$
0.0	1.97826	0.257895	0.000990	10.27	1.85
1.0	1.20566	0.185945	0.001231	10.58	2.17
2.0	0.433060	0.12177	0.0016051	10.75	2.51

Table 5 Maximum Radius b_{max} (Km) and Maximum Mass M_{max} (M_{\odot}) for B_g =57.55 MeV/fm³ taking L=0.1. L=0.3

taking E=0.1, y=0.5						
β	α	$b_{max}(km)$	$M_{max}(M_{\odot})$	Umax		
0.5	0.5	13.50	2.66	0.2905		
1.5	1.5	13.83	3.23	0.3447		
2.5	2.5	13.74	3.78	0.4057		

Table 6 Maximum Radius $b_{max}(Km)$ and Maximum Mass $M_{max}(M_{\odot})$ for B_g =95.11 MeV/fm^3 taking L=0.1, J = 0.3

β	α	$b_{max}(km)$	$M_{max}(M_{\odot})$	u_{max}
0.5	0.5	10.50	2.07	0.2905
1.5	1.5	10.76	2.51	0.3447
2.5	2.5	10.69	2.94	0.4057

VIII. PHYSICAL ANALYSIS OF THE STAR

This section presents an examination of various physical parameters including metric potentials, radial pressure, transverse pressure, and pressure anisotropy. The parameter value for α and β were selected arbitrarily. The metric potential distributions as functions of radial distance are illustrated in Fgs.(3)-(5) for the compact stellar objects PSRJ1903+327, HERX 1, and VELA X 1. Analysis of these profiles reveals that the boundary condition $e^{\nu} = e^{-\lambda}$ is satisfied at the stellar surface, while at the central region (r=0), the metric component satisfies $e^{\lambda} = 1$. Conversely, the metric component e^{ν} exhibits distinct values at the stellar center. Figs.(6)-(11) illustrate the radial distributions of matter density ρ , radial pressure p_r , transverse pressure p_t , pressure anisotropy, electric field and charge density for the compact stellar objects PSRJ1903+327, HERX 1, and VELAX 1.The density profile presented in fig.6 demonstrates that for any given bag parameter value, the matter density exhibits its maximum value at the stellar center and undergoes monotonic decrease with increasing radial coordinate. Furthermore, it is evident that elevated bag parameter values correspond to enhanced central density values. For a specified value of Bg. Consistent with the density behavior, the central radial pressure demonstrates positive correlation with increasing Bg values. The transverse pressure profile displays similar characteristics, with maximum values occurring at the center and sys thematic reduction toward the stellar surface. The pressure anisotropy parameter exhibits distinctly different behavior, vanishing at the center and progressively increasing with radial distance, ultimately reaching its maximum magnitude at the stellar boundary. The radial pressure distribution exhibits analogous behavior, achieving its peak magnitude at the center and diminishing to zero at the stellar boundary.

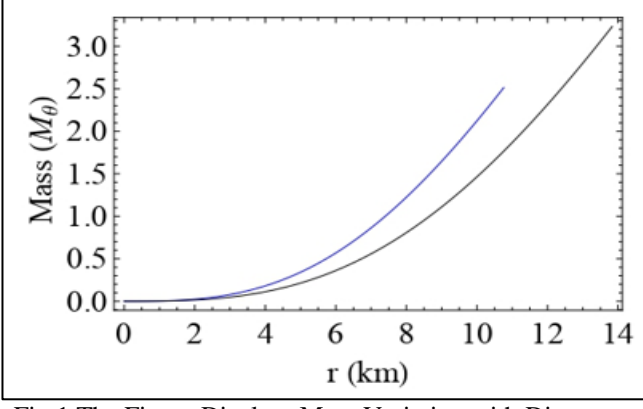


Fig 1 The Figure Displays Mass Variation with Distance r for Two Scenarios: Black Line (Bg =57.55MeV/ fm³, Radius=13.88km) and Blue Line (Bg=95.11MeV/ fm³, Radius=10.76km), with α = β =1.5

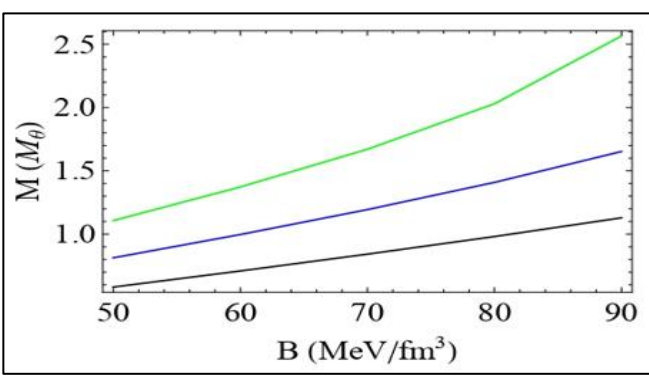


Fig 2 The Figure Displays Mass Variation with Bg Using Black (b=9km), blue (b=10km), and Green (b=11Km) Lines, with α = β =1.5.

IX. ENERGY CONDITIONS IN PRESENCE OF CHARGE

For a suitable and well behaved stellar model, all the energy conditions such as: (i) Null energy condition (NEC), (ii) Weak energy condition(WEC), (iii) Strong energy condition(SEC), (iv) Dominent energy condition (DEC) (49; 50) should be satisfied throughout interior of the star. The energy conditions are given below

- NEC: $\rho + p_r \ge 0$, $\rho + p_t + E^2 \ge 0$
- WEC: $\rho + p_r \ge 0$, $\rho + E^2/2 \ge 0$, $\rho + p_t + E^2 \ge 0$
- SEC: $\rho + p_r \ge 0$, $\rho + p_t + E^2 \ge 0$, $\rho + p_r + 2p_t + E^2 \ge 0$
- DEC: $\rho + E^2/2 \ge 0$, $\rho p_r + E^2 \ge 0$, $\rho p_t \ge 0$.

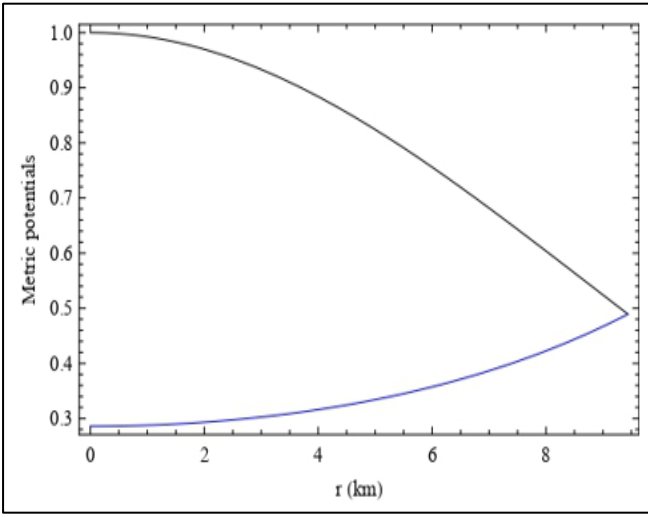


Fig 3 The Figure Displays Metric Potential Variation with Radial Distance r for Compact Object PSRJ1903+327, where α =2.5, β =1.5, L=0.1 and J=0.3. Blue Line Represents e^{ν} , Black Line Represents $e^{-\lambda}$.

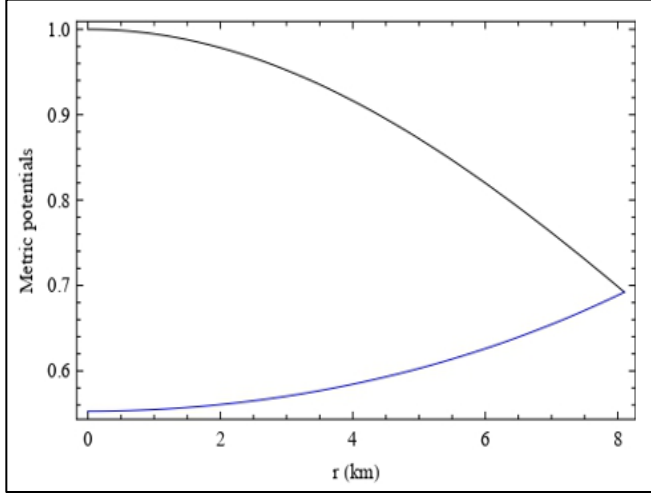


Fig 4 The Figure Displays Metric Potential Variation with Radial Distance r for Compact Object HER X-1, where α =2.5, β =1.5, L=0.1 and J=0.3. Blue Line Represents e^{ν} , black line represents $e^{-\lambda}$.

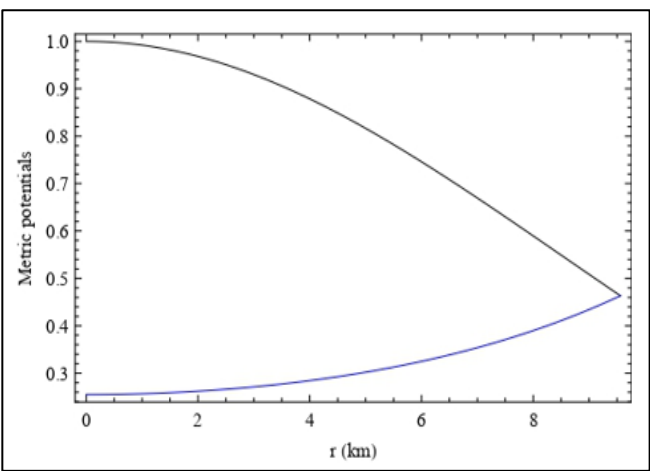


Fig 5 The Figure Displays Metric Potential Variation with Radial Distance r for Compact Object VELA X-1, where α =2.5, β =1.5, L=0.1 and J=0.3. Blue Line Represents e^{ν} , Black Line Represents e^{λ} .

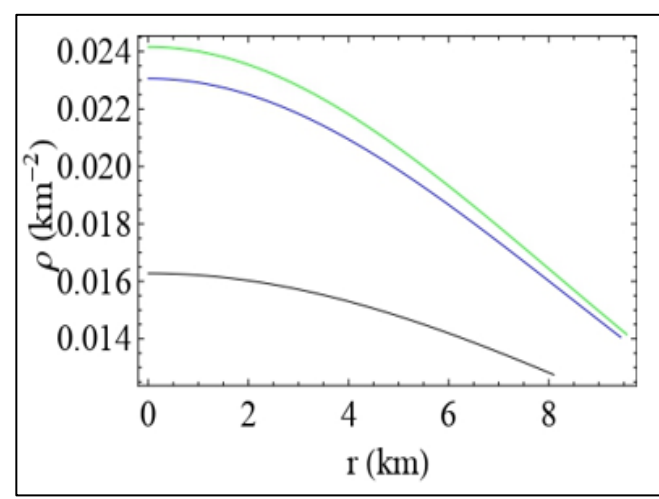


Fig 6 The Figure Displays Density Variation Versus Radial Distance r for Compact Objects PSRJ 1903+327 (Blue), HERX 1(Black), and VELAX 1(Green), with Parameters α =2.5, β =1.5, L=0.1 and J=0.3.

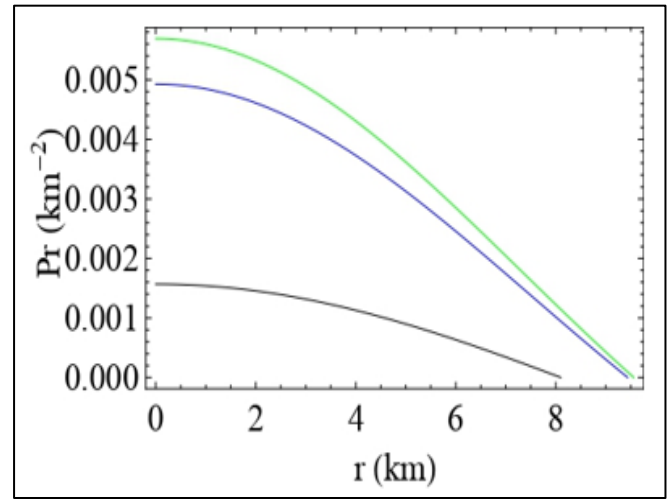


Fig 7 The Figure Displays Radial Pressure Variation Versus Radial Distance r for Compact Objects PSRJ 1903+327 (Blue), HERX 1(Black), and VELAX 1(Green), with Parameters α =2.5, β =1.5, L=0.1 and J=0.3.

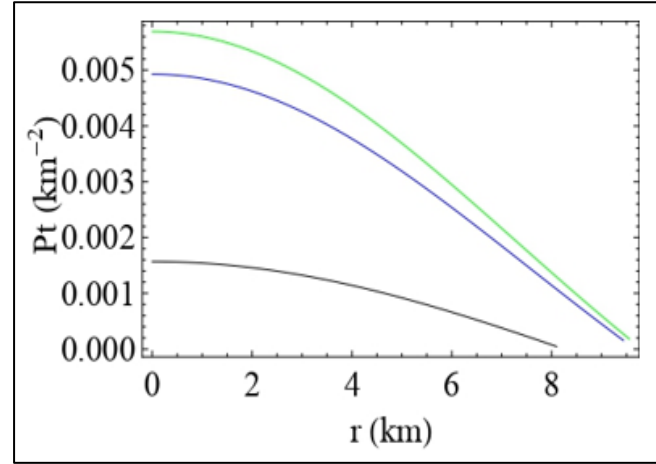


Fig 8 The Figure Displays Transverse Pressure Variation Versus Radial Distance r for Compact Objects PSRJ 1903+327 (Blue), HERX 1(Black), and VELAX 1(Green), with Parameters $\alpha = 2.5$, $\beta = 1.5$, L=0.1 and J=0.3.

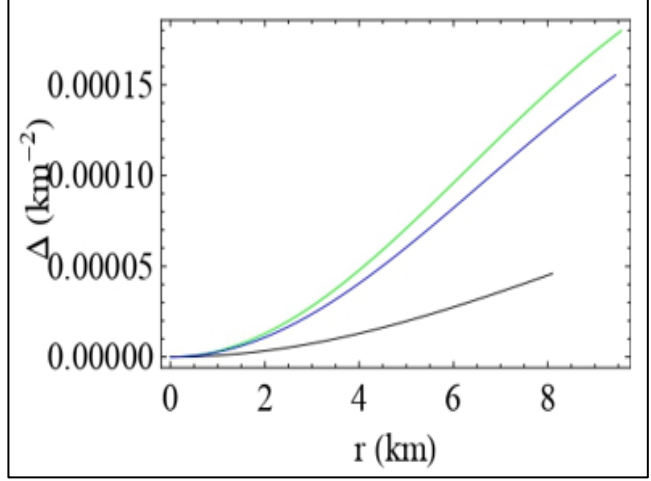


Fig 9 The Figure Displays Pressure Anisotropy Variation Versus Radial Distance r for Compact Objects PSRJ 1903+327 (Blue), HERX 1(Black), and VELAX 1(Green), with Parameters α =2.5, β =1.5, L=0.1 and J=0.3.

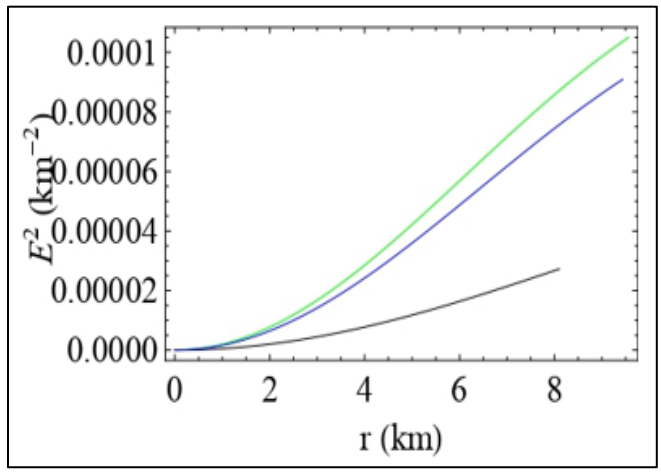


Fig 10 The Figure Displays Electric Field Variation Versus Radial Distance r for Compact Objects PSRJ 1903+327 (Blue), HERX 1(Black), and VELAX 1(Green), with Parameters α =2.5, β =1.5, L=0.1 and J=0.3.

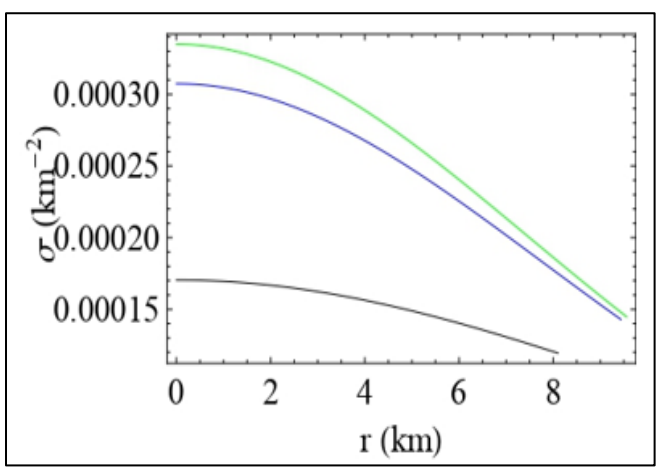


Fig 11 The Figure Displays Charge Density Variation Versus Radial Distance r for Compact Objects PSRJ 1903+327 (Blue), HERX 1(Black), and VELAX 1(Green), with Parameters α =2.5, β =1.5, L=0.1 and J=0.3.

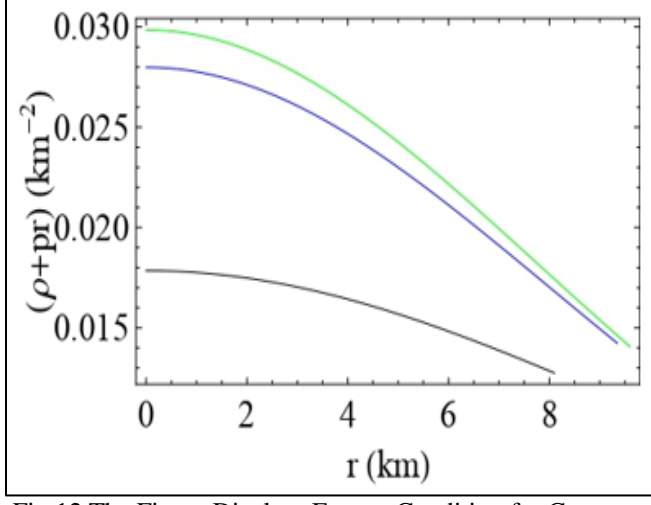


Fig 12 The Figure Displays Energy Condition for Compact Objects PSRJ 1903+327 (Blue), HERX 1(Black), and VELAX 1(Green), with Parameters α =2.5, β =1.5, L=0.1 and J=0.3.

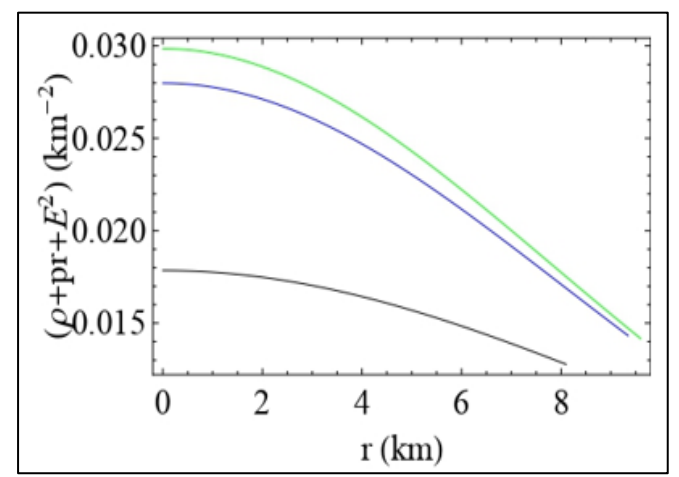


Fig 13 The Figure Displays Energy Condition for Compact Objects PSRJ 1903+327 (Blue), HERX 1(Black), and VELAX 1(Green), with Parameters α =2.5, β =1.5, L=0.1 and J=0.3.

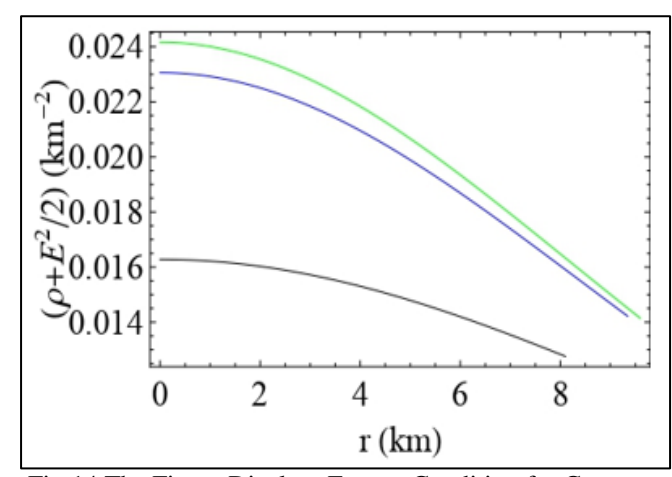


Fig 14 The Figure Displays Energy Condition for Compact Objects PSRJ 1903+327 (Blue), HERX 1(Black), and VELAX 1(Green), with Parameters α =2.5, β =1.5, L=0.1 and J=0.3.

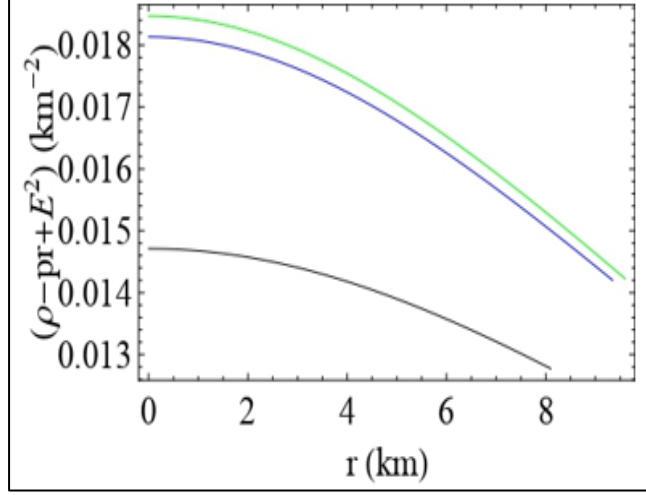


Fig 15 The Figure Displays Energy Condition for Compact Objects PSRJ 1903+327 (Blue), HERX 1(Black), and VELAX 1(Green), with Parameters α =2.5, β =1.5, L=0.1 and J=0.3.

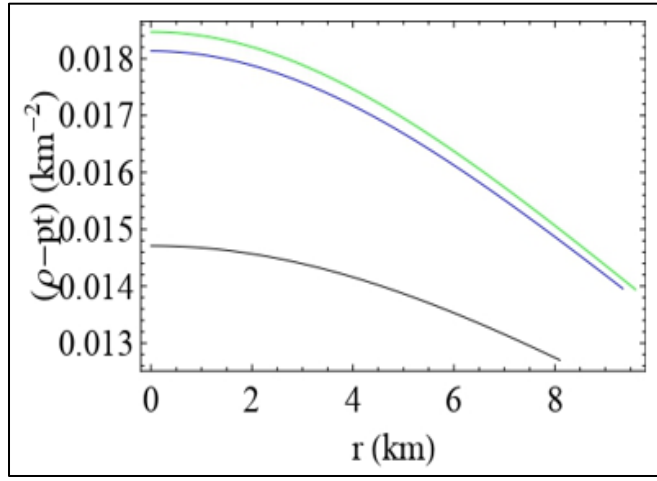


Fig 16 The Figure Displays Energy Condition for Compact Objects PSRJ 1903+327 (Blue), HERX 1(Black), and VELAX 1(Green), with Parameters α =2.5, β =1.5, L=0.1 and J=0.3.

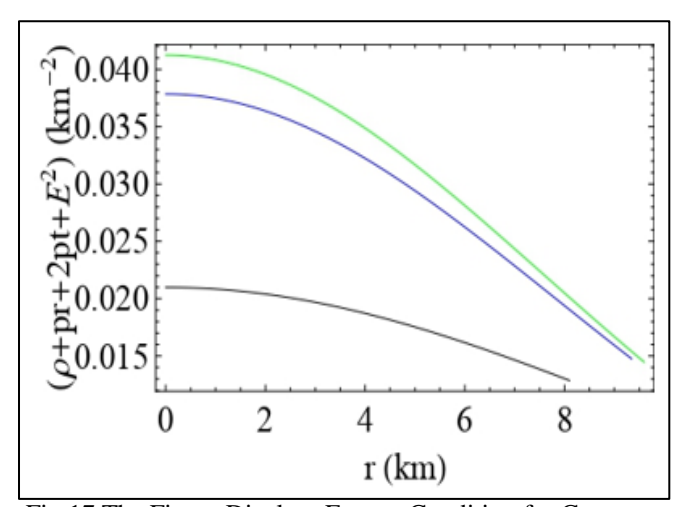


Fig 17 The Figure Displays Energy Condition for Compact Objects PSRJ 1903+327 (Blue), HERX 1(Black), and VELAX 1(Green), with Parameters α =2.5, β =1.5, L=0.1 and J=0.3.

Figs 12-17 show the different energy conditions. From these figures, it is evident that our model satisfy all energy conditions within the parameter space used to construct model.

X. CAUSALITYCONDITION

The fulfillment of causality condition is another important criterion which should satisfy to construct a well behaved stellar model. This condition tells us that the square of the radial sound speed (V_r^2) and the tangential sound speed (V_t^2) must obey the condition $V_r^2 = \frac{dp_r}{d\rho} \le 1$ and $V_t^2 = \frac{dp_t}{d\rho} \le 1$. In Figs. 18 and 19, we have shown the profile of causality conditions of compact objects PSRJ1903+327, HERX 1and VELAX 1. From the figures, it is evident that the square of the sound speeds throughout the interior of the star is less than 1 and also notice that both the speeds is

maximum at the center and monotonically decreasing away from the center.

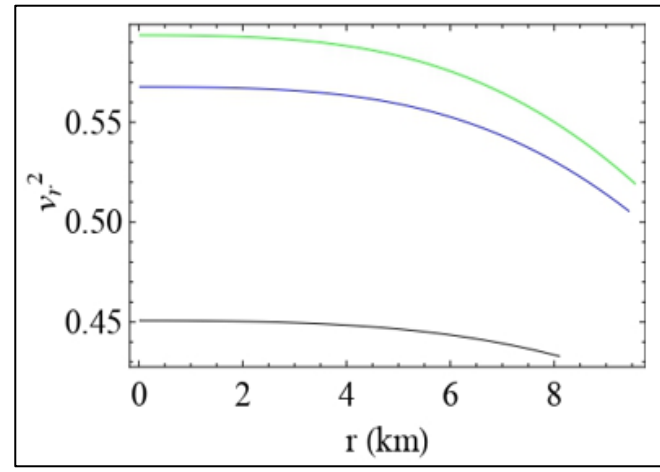


Fig 18 The Figure Displays Causality Condition for Compact Objects PSRJ 1903+327 (blue), HERX 1(Black), and VELAX 1(Green), with Parameters α =2.5, β =1.5, L=0.1 and J=0.3.

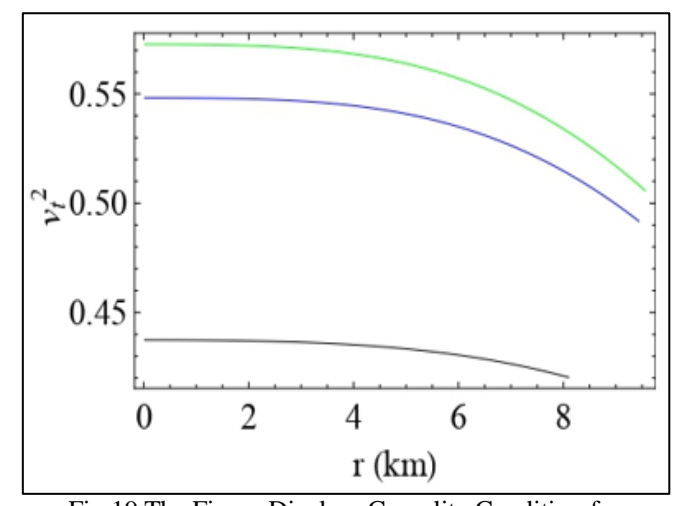


Fig 19 The Figure Displays Causality Condition for Compact Objects PSRJ 1903+327 (Blue), HERX 1(Black), and VELAX 1(Green), with Parameters α =2.5, β =1.5, L=0.1 and J=0.3.

XI. PHYSICAL APPLICATION OF THE MODEL

- In Order to Apply Physically, we have taken Three Compact Objects Namely:
- PSRJ1903+327(51) which has observed mass and radius $M=1.66M_{\odot}$ and b=9.438km respectively.
- The second compact object is HERX 1(52) which has observed mass and radius $M=0.85M_{\odot}$ and b=8.1km respectively.
- The third compact object is VELAX 1(54) which has observed mass and radius M=1.77M_☉ and b=9.56km respectively.

Using these three know compact objects, we have applied our model to study their physical properties. In Tab8, we have shown the values of central density, surface

density and central pressure of PSRJ1903+327, HERX 1and VELAX 1. In Table9, we have predicted the radius of two

compact stars GW170817 and GW190814.

Table 7 Values of Different Parameters of Compact Objects PSRJ1903+327, HERX 1 and VELAX 1 taking L=0.1, J=0.3, α =2.5 and β =1.5.

Star	Bg(MeV/fm ³)	A	H	h(km ⁻²)
PSRJ1903+327	105.38	-2.23788	0.285939	0.001051
HERX 1	95.60	-4.23418	0.552638	0.000583
VELAX 1	106.12	-1.95631	0.254986	0.001146

Table 8 Table Shows the Central Density $\rho(0)$, Central Pressure p(0) and Surface Density $\rho(s)$ for Different Star.

Compact	Bg (MeV/ fm ³)	$\rho(0)$	ρ(s)	p (0)
Star		(gm/cm ³)	(gm/cm ³)	(dyn/cm ²)
PSRJ1903+327	105.38	12.30x10 ¹⁴	7.49×10^{14}	$2.37x10^{35}$
HERX 1	95.60	8.68×10^{14}	6.80×10^{14}	7.54×10^{34}
VELAX 1	106.12	12.87x10 ¹⁴	7.55×10^{14}	2.74×10^{35}

Table 9 Prediction of Radius of Stars GW170817 (53) and GW190814 (54) Using Our Model. Here we have taken $\alpha = 1$

Compact	Observed	β	Predicted Radius(Km)		
Star	Mass(M)		Bg=57.55(MeV/fm³)	Bg=95.11(MeV/fm³)	
GW170817	1.4	0	11.32	9.48	
		0.5	11.30	9.45	
		1.0	11.27	9.43	
		1.5	11.25	9.40	
		2.0	11.22	9.37	
		2.5	11.20	9.34	
GW190814	2.59	0	13.47	11.11	
		0.5	13.40	11.01	
		1.0	11.33	10.92	
		1.5	11.26	10.84	
		2.0	11.19	10.75	
		2.5	13.13	10.67	

STABILITY OF THE MODEL: VARIATION OF LAGRANGIAN PERTURBATION OF PRESSURE WITH FREQUENCY

Recent studies examine stellar model stability using Lagrangian perturbation of radial pressure at stellar surfaces. Our model analyzes how Lagrangian perturbation of radial pressure varies with frequency (ω^2) by plotting pressure perturbation versus frequency (ω^2). In the present model, we employ the methodology established by Pretel (55), where in the radial oscillation mode is characterized through the following system of equations:

$$\frac{\mathrm{d}\chi}{\mathrm{d}r} = -\frac{1}{r} \left(3\chi + \frac{\Delta p_r}{\Gamma p_r} \right) + \frac{1}{2} \left(\frac{\mathrm{d}\nu}{\mathrm{d}r} \right) \chi, \dots \dots \dots \dots \text{eq}(40)$$

And

XII.

$$\chi(\frac{\omega^2}{C^2}e^{\lambda-\nu}(\rho+p_r)r-4\frac{dp_r}{dr}-\Sigma(\rho+p_r)e^{\lambda}rp_r+\frac{r}{4}(\rho+p_r)(\frac{d\nu}{dr})^2)$$

Where $\frac{8\pi G}{c^4} = \Sigma$, $\Gamma = \frac{dp_r}{dr}(\frac{\rho + p_r}{p_r})$ and the eigen function χ is connected to the radial part of the Lagrangian displacement by the relation $\chi = \frac{\delta(r)}{r}$. G is the Newtonian gravitational constant and C is velocity of light in free space. At the center of the star the eigen functions can be normalized so that $\chi(r=0)=1$. Again from Eq.(40), it is evident that this equation has a singularity at the center i.e at r=0. So, in order to find a realistic solution, the coefficient of $\frac{1}{r}$ must vanish as $r\to 0$ which gives the condition

$$\Delta p_r = -3\left(\frac{\lambda}{2}\right)\chi p_r, \dots eq(42)$$

Along with this condition, we have, at the surface of the star i.e at r=b the pressure is equal to zero and the Lagrangian perturbation of the pressure also vanishes i.e as $r \rightarrow b$

$$\Delta p_r = 0 \dots eq(43)$$

The absolute value of the Lagrangian change in pressure is plotted against frequency (ω_n^2) of compact objects PSRJ1903+327, HERX 1 and VELAX 1 and shown in Fig.20. The minima of these plots corresponds to correct value of the normal model frequency. It is evident that for all normal modes $(\omega_n^2) > 0$. Thus we can say that our model is stable under Lagrangian perturbation of radial oscillation.

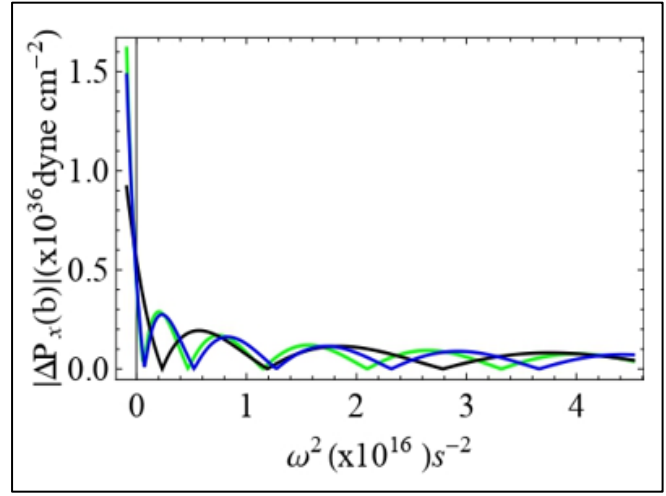


Fig 20 Figure Shows the Variation of Perturbation in Pressure with Frequency ω^2 of Compact Objects PSRJ1903+ 327, HERX 1 and VELAX 1. Blue Line for PSRJ1903+327, Black Line for HERX 1 and Green line for VELAX 1. Here α =2.5, β =1.5, L=0.1and J=0.3.

XIII. DISCUSSION

In this work, we have found a new solution of Einstein- Maxwell field equations using the g_{tt} component of metric potential stated in Eq. (12). In this paper, we have take n=6 for constructing our model. Using this value of g_{tt} for n = 6 we have obtained the value of g_{rr} component of metric potential both for isotropic and anisotropic charged star model. However solution for value n > 6 can also be obtained by taking suitable choice of pressure anisotropy as well as charge E². Using MIT bag EOS given in Eq. (3), we calculate the values of maximum mass and corresponding maxi mum radius by solving $\rho_s = 4B_g$ and p(b) = 0 for charged strange matter distribution. The values of maximum mass and maximum radius are shown in Tables 1-5. In these tables, we have shown different cases. In table 1, we have tabulated the values of maximum mass and maximum radius for different values of α with $\beta = 0$, J =0.3 and L=0.1 at Bg =57.55 MeV/ fm3 while in table. 2 for different values of β with $\alpha = 0$, J = 0.3 and L = 0.1 at Bg =57.55MeV/ fm³. Similarly in tables. 3 and 4, we have shown maximum mass and maximum radius at Bg = 95.11 MeV/ fm³. From the table it is evident that for an isotropic uncharged star the maximum mass and radius is obtained as $b_{max} = 13.21$ Km and $M_{max} = 2.38$ M $_{\odot}$ for Bg = 57.55 MeV/ fm³ and $b_{max} = 10.27$ Km and $M_{max} = 1.85$ M_{\odot} for Bg = 95.11 MeV/ fm³. The maximum mass and radius at two different bag values with non zero α and β are shown in Tables 5 and 6. The maximum compactness are shown in Tables 5 and 6. we have shown the maximum compactness and surface red shift. Central density, surface density and central pressure of compact stars PSRJ1903+327, HER X 1 and VELA X 1 are shown in Table 8. Fig. 1 shows the variation of mass function with radial distance. From this figure, it is evident that mass function is well behaved and it vanishes at the center of the star. The profile of mass variation with bag value for different radius is shown in Fig. 2. In Figs. 3-5, we have shown the variation of metric potentials with distance of compact objects PSRJ1903+327,

https://doi.org/10.38124/ijisrt/25sep1255

HERX 1 and VELAX 1. From these figures, It is evident that the value of $e^{-\lambda} = e^{\nu}$ at r = b. In Fig. 6, we have shown the variation of density with respect to distance of stars PSRJ1903+327, HER X 1 and VELAX 1. It is evident that the density is maximum at the centre and decreases away from the centre. The variation of radial and transverse pressure are shown in Figs. 7 and 8. Radial pressure is maximum at the center and decreases to zero at the surface. The profile of pressure anisotropy of compact objects PSRJ1903 + 327, HERX 1 and VELAX 1 are shown in Fig.9. From the figure it is evident that the pressure anisotropy vanishes at the center. The variation of electric field with radial distance of stars PSRJ1903 + 327, HER X 1 and VELA X 1 is shown in Fig. 10. All the energy conditions are well satisfied in our model and shown in Figs. 12-17. From the figures, it is evident that the model follows the energy conditions. In Figs. 18 and 19, we have shown the profile of square of radial sound speed and transverse speed with distance of compact objects PSRJ1903+327, HER X 1 and VELAX 1. In this model, we have studied the stability by showing the variation in the absolute value of the Lagrangian perturbation of radial pressure at the surface of the compact stars PSRJ1903+327, HER X 1 and VELA X 1 with the frequencies of the normal mode of oscillations and The variation of absolute value of Lagrangian perturbation in radial pressure at the surface against ω^2 is shown in Fig. 20. We note that all cases, the frequency spectrum is real $(\omega_n^2) > 0$). This immediately indicates that our model is stable under this criterion.

REFERENCES

- [1]. Lugones, G. and Arbail, J.D.V.:Phys. Rev. D 95, 064022 (2017)
- [2]. Brilenkov, M., et al.: JCAP08,002(2013)
- [3]. Arbail, J.D.V. and Malheiro, M.: JCAP11, 012 (2016)
- [4]. Paulucci,L.andHorvath,J.E.:Phys.Lett.B733,1 64 (2014)
- [5]. Chowdhury, S.R., et al.: Int. J. Mod. Phys. D 29, 2050001 (2020)
- [6]. Kapusta, J.: Finite Temperature Field Theory, (Cambridge Univ. Press), p. 163-165 (1994)
- [7]. Madsen, J.: Lect. Notes Phys., 516, 162, (1999)
- [8]. Farhi, E. and Jaffe, R. L.: Phys. Rev., D 30, 2379, (1984)
- [9]. Ruderman, R.:Astron. Astrophys., 10, 427 (1972)
- [10]. Canuto, V.:Ann. Rev. Astron. Astrophys., 12, 167 (1974)
- [11]. Bowers, R. and Liang, E.:Astrophys. J., 188, 657 (1974)
- [12]. Kippenhahn, R. A.: Weigert, Steller Structure and Evolution (Springer, Berlin, 1990)
- [13]. Herrera, L. and Santos, N.O.: Phys. Report., 286,53 (1997)
- [14]. Sawyer, R. F.: Phys. Rev. Lett., 29, 382 (1972)
- [15]. Sokolov, A. I.:J. Exp. Theo. Phys., 79, 1137 (1980)
- [16]. Mak, M. K. and Harko, T.:Chin. J. Astron. Astrophys., 2, 248 (2002)

- [17]. Maharaj, S.D. and Marteens, R.:Gen. Rel. Grav., 21, 899(1989)
- [18]. Gokhroo, M. K. and Mehra, A.L.:Gen. Rel. Grav., 26, 75 (1994)
- [19]. Dev, K. and Gleiser, M.:Gen. Rel. Grav., 35, 1435.(2003)
- [20]. Dev,K. and Gleisser,M.:Int.J.Mod.Phys.,D13,1389,(2004)
- [21]. Bayin, S.S.: Physical Review, D 26, 1262-1274 (1982)
- [22]. Krori, K.D., Borgohaiann, P. and Devi, R.:Canadian Journal of Physics,62,239-246(1984)
- [23]. Herrera,L.and PoncedeLeon,:J.JournalofMath.Phys.,26,2302-2307(1985)
- [24]. Bondi, H.:Mon. Not. R. Astron. Soc., 259, 365-368 (1992)
- [25]. Bhar,P.and Ratanpal,B.S.:Astrophys.Space.Sci.,361,217(201 6)
- [26]. Bonnor, W.B.: Mon. Not. R. Astron. Soc. 29,443-446 (1965)
- [27]. Rosseland, S.:Mon. Not. R. Astron. Soc., 84, 720 (1924)
- [28]. Whitman, P.G. and Burch, R.C.:Phys. Rev., D 24, 2049-2055(1981)
- [29]. De Felice,F.,Yu,Y.and Fang,J.:Mon.Not.R.Astron. Soc., 277, L17-L19 (1995)
- [30]. Ivanov, B.V.: Phys. Rev., D65, 104001 (2002)
- [31]. Rahaman,F.,et al.:Astrophys.SpaceSci.,331,191-197 (2011)
- [32]. Bijalwan, N.:Astrophys. Space. Sci., 336, 485489 (2011)
- [33]. Pant,N.and Rajasekhara,S.:Astrophys.SpaceSci.,333,161-168(2011)
- [34]. Pandya, D.M., Thomas, V.O. and Sharma, R.:Astrophys.Space Sci., 356, 285 (2015)
- [35]. Thirukkanesh, S. and Ragel, F.C.: Astrophys. Space Sci., 354, 415 (2014)
- [36]. Buchdahl,H.A.:Phys.Rev.,116,1027,(1959)
- [37]. Tolman, R.C.: Phys. Rev., 55, 364, (1939)
- [38]. Kuchowicz,B.:Astrophys.Space.Sci.,33,L13(1 975)
- [39]. Adler, R.:J. Math. Phys., 15, 727 (1974)
- [40]. Adams,R.C.and Cohen,J.M.:Astrophys.J.,198,507 (1975)
- [41]. Durgapal, M.C.: J. Phys., A15, 2637 (1982)
- [42]. Sunzu,J.M.and Danford,P.:PramanaJ.Phys.,89,44 (2017)
- [43]. Sunzu, J.M., Maharaj, S.D. and Ray, S.:Astrophys. Space Sci., 354, 517 (2014)
- [44]. Sarkar, S. et al.: Astrophys. Space Sci., 369, 19(2024)
- [45]. SarkarS,et al.:Int.J.Geom.Meth.Mod.Phys.,12,41 (2025)
- [46]. Sarkar.,S. A J. Planetary.Space. Sci. 4(3): 150 (2025)
- [47]. Reissner, H.: Ann. Phys., 50, 106(1916)

https://doi.org/10.38124/ijisrt/25sep1255

- [48]. Nordstrm, G.:Verhandl. Koninkl. Ned. Akad.Wetenschap.,Afdel. Natuurk.,26, 1201 (1918)
- [49]. Brassel,B.P.,Maharaj,S.D., and Goswami,R.:Prog. Theor. Exp. Phys., 103-E01 (2021)
- [50]. Maeda, H. and Martinez, C.:Prog. Theor. Exp. Phys., 043- E02 (2020)
- [51]. Güver, T., Wroblewski, P., and Camarota, L., et al .: Astro-phys. J, 719, 1807 (2010)
- [52]. Gangopadhyay, T., Ray, S., X.-D. Li, J. Dey, and Dey, M.,: Mon. Not. R. Astron. Soc., 431, 3216 (2013)
- [53]. Bauswein, A., Bastian, N.F., Blaschke, D., Chatzii on-nou, K., Clark, J.A., Fischer, T., Janka, H., Just, O., Oertel, M., and Steriouslas, N.: AIP Conference Proceedings, 2127, 020013 (2019)
- [54]. Abbott,R.,etal.:ApJL896,L44(2020)
- [55]. Pretel, J.M.Z.: Eur. Phys. J. C80, 726 (2020)